Applied Catalysis B: Environmental 94 (2010) 134–141

Contents lists available at ScienceDirect

Applied Catalysis B: Environmental

journal homepage: www.elsevier.com/locate/apcatb

# Integration of C–C coupling reactions of biomass-derived oxygenates to fuel-grade compounds

Elif I. Gürbüz, Edward L. Kunkes, James A. Dumesic *

*Department of Chemical and Biological Engineering, University of Wisconsin, Madison, WI 53706, USA*

ARTICLE INFO

*Article history:*
Received 26 August 2009
Received in revised form 22 October 2009
Accepted 2 November 2009
Available online 10 November 2009

*Keywords:*
Aldol condensation
Ceria
Zirconia
$CO_2$ inhibition
Water inhibition

ABSTRACT

Ceria-zirconia mixed oxides with different compositions including pure ceria and pure zirconia were prepared and characterized using temperature-programmed desorption (TPD) of $CO_2$ and $NH_3$, X-ray diffraction (XRD), and BET surface area measurements. Bi-functional catalysts for C–C coupling of ketones by aldol condensation/hydrogenation were prepared by depositing palladium on these ceria-zirconia mixed oxides, and these catalysts were studied for the conversion of 2-hexanone, a representative ketone that can be derived from sugars in biomass. The $Pd/ZrO_2$ catalyst showed the best resistance to inhibition by $CO_2$, an important factor in catalyst performance because of the presence of $CO_2$ in biomass-derived feed streams. Furthermore, this catalyst displayed high activity for aldol condensation, as well as good resistance to inhibition by water. These properties make $Pd/ZrO_2$ a desirable catalyst for integration in a single reactor of aldol condensation/hydrogenation reactions with ketonization processes, the latter of which convert carboxylic acids to ketones plus $CO_2$ and $H_2O$. The feasibility of this integration was studied with the mixture of a carboxylic acid (butanoic acid) and a ketone (2-hexanone) in a double bed system, and the integrated process showed high activity as well as selectivity to C–C coupling products.



## 1. Introduction

Concerns about diminishing reserves of petroleum resources and issues related to climatic consequences of the accumulation of $CO_2$ in the atmosphere have prompted the development of renewable and carbon-neutral alternative sources of energy, such as biomass. Carbohydrates derived from biomass can be converted to fuel-grade products such as light alkanes ($C_1$–$C_4$), branched alkanes ($C_6$–$C_{12}$), linear or singly branched alkanes ($C_7$–$C_{12}$), benzene and substituted aromatics by a series of catalytic processes demonstrated in our recent work [1]. These conversion processes are initiated by de-oxygenation of sugars or polyols over a Pt-Re bi-metallic catalyst supported on carbon to obtain a hydrophobic mixture of mono-functional species, such as carboxylic acids, ketones, alcohols and heterocycles with carbon numbers ranging from 4 to 6. The maximum carbon chain length of these species is limited to the carbon number of the sugar or polyol feed. However, higher molecular weight alkanes are required for gasoline, diesel and jet fuel, and for this purpose the hydrophobic mixture has to be subjected to C–C coupling reactions [1].

Two important coupling reactions for the upgrading of mono-functional oxygenated compounds for transportation fuel applications are ketonization and aldol condensation/hydrogenation. In ketonization reactions, two carboxylic acid molecules combine to form a higher molecular weight linear ketone, $CO_2$ and water [2], whereas in aldol condensation/hydrogenation reactions, two ketone or secondary alcohol molecules couple to form a heavier branched ketone [3]. These ketones obtained can then be converted into corresponding fuel-grade alkanes by dehydration/hydrogenation over bi-functional solid-acid supported noble metal catalysts such as $Pt/NbOPO_4$ [4]. It was found in our previous work that ketonization must be performed prior to aldol condensation/hydrogenation, because the active basic sites in the aldol condensation catalyst are poisoned by the presence of carboxylic acids [1,5]. Carboxylic acids in the hydrophobic mixture can be ketonized with nearly 100% yield over a $Ce_1Zr_1O_x$ mixed-oxide catalyst at temperatures from 623 to 673 K [1]. The aldol condensation/hydrogenation was carried out over $Pd/Ce_1Zr_1O_x$ with $H_2$ co-feed. Metal catalyzed hydrogenation of the unsaturated dehydrated aldol condensation product is required to overcome the equilibrium limitation of aldol condensation reaction and obtain high yields [3]. In addition, metal functionality is needed to catalyze the dehydrogenation reaction of alcohols to form ketones for coupling reactions [6].

In a recent work, we have suggested that ketonization and aldol condensation/hydrogenation reactions could be integrated in a single reactor with a double bed system, because the reaction conditions for both reactions are similar. Integrating the ketoniza-

* Corresponding author. Tel.: +1 608 2621095; fax: +1 608 2625434.
*E-mail address:* dumesic@engr.wisc.edu (J.A. Dumesic).

0926-3373/$ – see front matter © 2009 Elsevier B.V. All rights reserved.
doi:10.1016/j.apcatb.2009.11.001

tion and aldol condensation steps into a single reactor system would streamline the overall C–C coupling process. However, the $CO_2$ produced in the ketonization reaction is a known poison for basic sites active in aldol condensation [7,8]. We have shown in our previous work [9] that the presence of 5% $CO_2$ in the feed is detrimental to aldol condensation activity (~90% decrease in activity) over $Pd/Ce_1Zr_1O_x$. Accordingly, we concluded that it was beneficial to remove $CO_2$ prior to the aldol condensation/hydrogenation step over $Pd/Ce_1Zr_1O_x$.

It has been shown in literature that the nature of the interaction of $CO_2$ with the oxide surface can be modified by changing the composition of mixed oxides [10,11]. In this current work, we study the possibility of modifying the composition of ceria-zirconia mixed oxide to formulate an aldol condensation catalyst that is not severely inhibited by $CO_2$, so as to permit the integration of ketonization and aldol condensation reactions in a single reactor. In addition to $CO_2$ inhibition, inhibition by water also needs to be investigated, because water is a by-product of ketonization as well as aldol condensation. For example, we have shown in our recent work that a 40% decrease in activity takes place for aldol condensation of 2-butanone over $Pd/Ce_1Zr_1O_x$ when a mixture containing 12 wt% water in 2-butanone is used as the feed [9].

## 2. Experimental

### 2.1. Catalyst preparation

Ceria-zirconia mixed oxides with different molar compositions were prepared via co-precipitation of $Ce(NO_3)_3$ and $ZrO(NO_3)_2$ with $NH_4OH$ (Aldrich) according to Serrano-Ruiz et al. [12] with appropriate concentrations to obtain desired Ce/Zr ratios. The $Pd/Ce_aZr_bO_x$ catalysts were prepared via incipient wetness impregnation of $Ce_aZr_bO_x$ with an amount of aqueous solution of $Pd(NO_3)_2$ (Aldrich) necessary to obtain the nominal metal loading of 0.25 wt%. The catalysts were dried in air at 373 K overnight and calcined in air at 623 K for 2 h.

### 2.2. Reaction kinetics studies

2-Hexanone and butanoic acid were purchased from Sigma–Aldrich and used without further purification. Hydrogen (99%) and 10 mol% $CO_2$ in $H_2$ were purchased from Airgas and used without further purification. The conversions of 2-hexanone over $Pd/Ce_aZr_bO_x$ were carried out at 598 and 623 K, pressure of 5 bar, and liquid flow rates of 0.08 and 0.16 mL/min. The molar ratio of the gas flow rate to the liquid flow rate was maintained at 5.5. A fixed bed, down-flow reactor consisting of a half-inch stainless steel tube was used for all experiments. Quartz wool was used in the lower end of the reactor to keep the catalyst bed in place. The catalyst was mixed with crushed fused $SiO_2$ granules (Aldrich) in a 2:1 volumetric ratio to maintain bed height. The reactor was heated with an aluminum block that was heated externally by a well-insulated furnace (Applied Test Systems). Type-K thermocouples (Omega) were used to measure the reaction temperature, which was controlled by a PID controller (Love Controls) connected to a variable transformer (Tesco). Mass flow controllers (Brooks 5850E) were used to regulate the flow of $H_2$ and $CO_2$ (10 mol% in $H_2$) during the experiments. The liquid feed was pumped from a graduated cylinder by an HPLC pump (Lab Alliance series 1) to a needle located at the entrance of the catalyst bed. A back-pressure regulator (GO model BP-60) was used to control the total pressure, which was measured by two gauges at the entrance and the exit of the bed. A gas–liquid separator at room temperature was used to collect the liquid effluent phase for analysis. The catalysts were reduced in situ at 623 K (ramp rate of 0.5 K $min^{-1}$) for 2 h in flowing $H_2$ (200 $cm^3$(STP) $min^{-1}$). After the reduction was completed, the temperature and pressure were adjusted and the feed flow was started with flowing $H_2$ or $H_2$–$CO_2$ mixtures. The weight hourly space velocity (WHSV) was calculated for experiments using the mass flow rate of the liquid flow into the reactor and the mass of the catalyst used.

Experiments employing a double bed, single reactor configuration were performed in a fixed bed, down-flow reactor system consisting of a half-inch stainless steel tube. In contrast to the single bed experiments, two different catalysts (2 g each) were loaded in the same reactor, separated by whole fused $SiO_2$ granules. $Pd/ZrO_2$ catalyst was placed on the quartz wool and fused $SiO_2$ granules were placed on top of this bed. $Ce_1Zr_1O_x$ catalyst was then placed on the silica granules, so that the feed could pass through the ketonization catalyst first and the aldol condensation/hydrogenation catalyst second. Both catalysts were mixed with crushed fused $SiO_2$ granules (Aldrich) in a 1:1 volumetric ratio.

The rate of gas production was measured with a bubble flow meter. An HP GC5890 gas chromatograph, equipped with a Haysep DB 100/120 column (Alltech) and thermal conductivity detector (TCD), was used to quantify CO and $CO_2$, and an Agilent GC6890, equipped with an Rtx column (Agilent) and a flame ionization detector (FID), was used to quantify gas-phase alkanes. Liquid phase analysis was performed with a Shimadzu GC 2060, equipped with a DB-5 column (Restek) and an FID detector and a Shimadzu 2060 GC/MS with a NIST library of spectra. Liquid and gas analysis points were collected every 2–3 h, and steady state was usually achieved after 6 h time-on-stream. At our reaction conditions, 2-hexanol was in equilibrium with 2-hexanone; therefore, the conversion of 2-hexanone to 2-hexanol was not factored into the total conversion calculation, as given by Eq. (1). The selectivities to reaction products were calculated on a molar carbon basis, as given by Eq. (2). In Eqs. (1) and (2), $R$ represents the molar flow rate, $f$ represents reactant conversion, $S$ represents the carbon selectivity, and $N$ is the carbon number of a given species. All carbon balances closed to within 10%.

$$f_{\text{2-hexanone}} = \left(1 - \frac{R_{\text{2-hexanone\_out}} + R_{\text{2-hexanone\_out}}}{R_{\text{2-hexanone\_in}}}\right) \times 100\% \quad (1)$$

$$S_j = \left(\frac{R_{j\_\text{out}} N_j}{\sum_j (R_{j\_\text{out}} N_j)}\right) \times 100\% \quad (2)$$

### 2.3. Catalyst characterization

#### 2.3.1. BET and XRD measurements

The BET surface area was measured by nitrogen adsorption at liquid nitrogen temperature using a standard volumetric apparatus [13]. X-ray diffraction (XRD) was used to investigate the phase structure of the $Pd/Ce_aZr_bO_x$ catalysts. A Scintag PAD V X-ray diffractometer with a monochromated $CuK_\alpha$ X-ray tube was used in the diffraction studies. The tube voltage and current were 45 kV and 40 mA, respectively. Diffraction patterns were collected in the 20–65° $2\theta$ range, with 0.01° intervals and a dwell time of 2 s.

#### 2.3.2. Temperature-programmed desorption (TPD) experiments

Carbon dioxide and ammonia temperature-programmed desorption (TPD) experiments were carried out using an apparatus consisting of a mass flow controller (Teledyne-Hastings) and a tube furnace connected to a variable power-supply and PID temperature controller (Love Controls) with a K-type thermocouple (Omega). The gas effluent was monitored by a mass spectrometer system consisting of a quadruple residual gas analyzer (Stanford Instruments RGA 200) inside a vacuum chamber. Vacuum was provided by a diffusion pump connected in series to a rotary pump.

The effluent was introduced into the vacuum chamber via a constricted quartz capillary, resulting in a pressure of $5 \times 10^{-5}$ Torr inside the chamber. Dried, unreduced catalyst samples were loaded into a 12.6 mm (0.5 in.) outer diameter, fritted quartz tube reactor. Prior to desorption experiments, 0.3–1 g of catalyst was reduced in flowing hydrogen (100 $cm^3$(STP) $min^{-1}$) for 2 h at 623 K. The catalyst was degassed for 1 h in flowing helium (200 $cm^3$(STP) $min^{-1}$) at the reduction temperature, and then cooled to 300 K for $CO_2$ adsorption and 423 K for $NH_3$ adsorption, respectively. Carbon dioxide was adsorbed onto the reduced catalysts by exposure to flowing 10 mol% $CO_2$ in helium (100 $cm^3$(STP) $min^{-1}$) for 30 min. Residual $CO_2$ was removed by purging the catalyst with helium (200 $cm^3$(STP) $min^{-1}$) at 300 K for 2 h. Ammonia adsorption was performed in a similar manner as $CO_2$ adsorption, except that both adsorption and purging steps were performed at 423 K, and a 1 mol% $NH_3$ in He gas mixture was used. Desorption of $CO_2$ or $NH_3$ was performed by heating the catalyst at a rate of 10 K $min^{-1}$ under flowing helium (50 $cm^3$(STP) $min^{-1}$) from room temperature to 1073 K for $NH_3$ or 1123 K for $CO_2$.

## 3. Results and discussion

### 3.1. Surface and bulk characterization

The desorption profiles of $NH_3$ and $CO_2$ from several Pd-supported ceria-zirconia catalysts of varying compositions, as well as pure $CeO_x$ and $ZrO_2$, are shown in Figs. 1 and 2, respectively. These profiles were integrated to obtain the quantities of acidic and basic surface sites per gram of catalyst, which are reported in Table 1. The BET surface areas are also listed in Table 1. The surface area increases significantly upon the addition of zirconia to ceria, and remains nearly constant when comparing the mixed oxides with pure zirconia. Fig. 1 and Table 1 show that the number of surface acidic sites increases with zirconia content. $Pd/CeO_x$ shows no appreciable surface acidity, as measured by TPD, while $Pd/ZrO_2$ has the maximum number of surface acid sites (212 μmol/g-cat or 1.4 μmol/$m^2$). Furthermore, the $NH_3$ desorption profiles of all catalysts display a single uniform peak in the range of 560–600 K. These results suggest that surface acidity is associated primarily with $ZrO_2$.

The $CO_2$ desorption profiles in Fig. 2 show the presence of basic sites of varying $CO_2$ adsorption strength for different ceria/zirconia molar ratios. These profiles can be divided into three distinct regions representing weak adsorption sites (300–500 K), medium-strength adsorption sites (500–700 K), and strong adsorption sites (700–1000 K) [14]. The total numbers of $CO_2$ binding sites are given in Table 1 and the distributions of weak, medium and strong $CO_2$ binding sites are given in Table 2. According to the literature [10,14], the weak sites for $CO_2$ binding are associated with the formation of hydrogencarbonates due to surface $OH^-$ groups; the medium-strength sites are associated with $M^{x+}\cdots O^{2-}$ pairs and the formation of bridged and bidentate carbonates; and the strong binding sites are associated with low coordination $O^{2-}$ ions and the formation of more strongly bound carbonates. All these species have been identified by FTIR studies of $CO_2$ adsorbed on ceria-zirconia mixed-oxide catalysts together with pure ceria and zirconia by Daturi et al. [15]. According to our TPD results, strong $CO_2$ binding sites are associated with ceria only, since these sites gradually disappear as the $ZrO_2$ content increases, as shown in Table 2, whereas $ZrO_2$ possesses only weak and medium-strength adsorption sites associated with $OH^-$ and $M^{x+}\cdots O^{2-}$ pairs. The mixed-oxide catalysts show similar desorption profiles, and possess a mixture of weak, medium and strong (low coordination

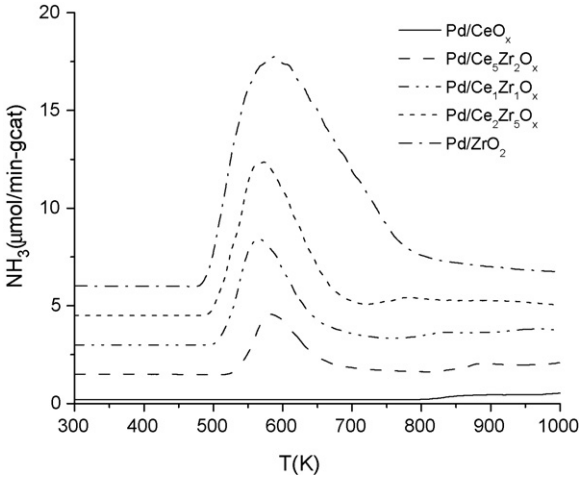


**Fig. 1.** TPD of $NH_3$ on $Pd/CeO_x$, $Pd/Ce_5Zr_2O_x$, $Pd/Ce_1Zr_1O_x$, $Pd/Ce_2Zr_5O_x$ and $Pd/ZrO_2$. Site counts are presented with increasing offsets for clarity.

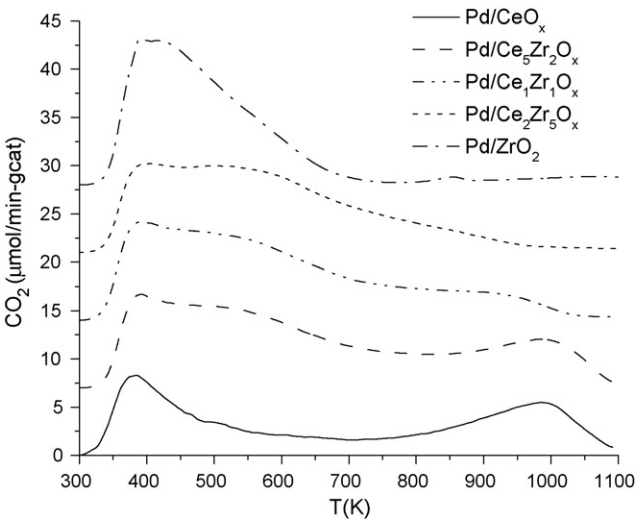


**Fig. 2.** TPD of $CO_2$ on $Pd/CeO_x$, $Pd/Ce_5Zr_2O_x$, $Pd/Ce_1Zr_1O_x$, $Pd/Ce_2Zr_5O_x$ and $Pd/ZrO_2$. Site counts are presented with increasing offsets for clarity.

**Table 1**
Quantification of basic and acidic sites and BET surface areas of 0.25 wt% $Pd/CeO_x$, $Pd/Ce_5Zr_2O_x$, $Pd/Ce_1Zr_1O_x$, $Pd/Ce_2Zr_5O_x$ and $Pd/ZrO_2$.

| Catalyst | $CO_2$ (TPD) (μmol/g) | $NH_3$ (TPD) (μmol/g) | BET area ($m^2$/g) |
|---|---|---|---|
| 0.25 wt% $Pd/CeO_x$ | 266 | 0 | 88 |
| 0.25 wt% $Pd/Ce_5Zr_2O_x$ | 414 | 27 | 131 |
| 0.25 wt% $Pd/Ce_1Zr_1O_x$ | 380 | 54 | 133 |
| 0.25 wt% $Pd/Ce_2Zr_5O_x$ | 350 | 86 | 141 |
| 0.25 wt% $Pd/ZrO_2$ | 296 | 212 | 149 |

**Table 2**
Quantification of weak, medium-strength and strong $CO_2$ binding sites over 0.25 wt% $Pd/CeO_x$, $Pd/Ce_5Zr_2O_x$, $Pd/Ce_1Zr_1O_x$, $Pd/Ce_2Zr_5O_x$ and $Pd/ZrO_2$.

| Catalyst | $CO_2$ (μmol/g) | | |
|---|---|---|---|
| | Weak ($T < 500$ K) | Medium ($500 < T < 700$ K) | Strong ($T > 700$ K) |
| 0.25 wt% $Pd/CeO_x$ | 95 | 45 | 126 |
| 0.25 wt% $Pd/Ce_5Zr_2O_x$ | 131 | 134 | 149 |
| 0.25 wt% $Pd/Ce_1Zr_1O_x$ | 142 | 139 | 99 |
| 0.25 wt% $Pd/Ce_2Zr_5O_x$ | 129 | 150 | 71 |
| 0.25 wt% $Pd/ZrO_2$ | 195 | 101 | 0 |

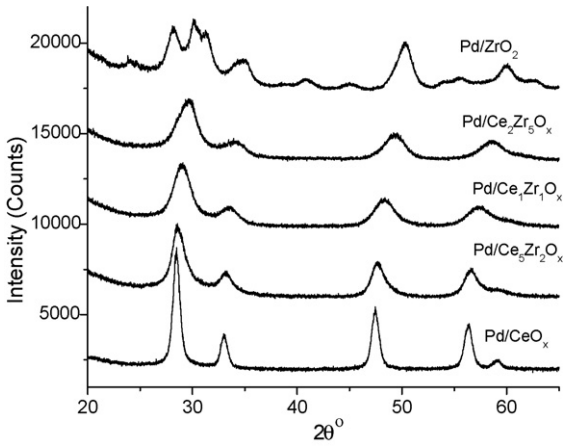


**Fig. 3.** XRD patterns for $Pd/CeO_x$, $Pd/Ce_5Zr_2O_x$, $Pd/Ce_1Zr_1O_x$, $Pd/Ce_2Zr_5O_x$ and $Pd/ZrO_2$. Counts are presented with increasing offsets for clarity.

$O^{2-}$ ions) binding sites. It is interesting to note that the mixed-oxide catalysts possess a greater number of intermediate strength binding sites than either $Pd/CeO_x$ or $Pd/ZrO_2$. The presence of the aforementioned distribution of $CO_2$ binding sites on $Ce_2Zr_5O_x$, $Ce_1Zr_1O_x$ and $Ce_5Zr_2O_x$ surfaces likely results from surface heterogeneity introduced by substituting Ce ions with $Zr^{4+}$ ions. The addition of Zr to Ce increases the mobility of $O^{2-}$ ions in the lattice [12,16], and is therefore likely to cause a higher number of $O^{2-}$ sites that bind $CO_2$ more strongly. It is important to note that the acid and base properties can be attributed to the metal oxide supports, since we have shown in our previous work with TPD experiments that the presence of 0.25 wt% Pd does not change the acid or base properties of $Ce_1Zr_1O_x$ [9].

The XRD patterns collected after calcination of catalysts consisting of 0.25 wt% Pd supported on ceria-zirconia mixed oxides with different compositions are shown in Fig. 3. The fluorite cubic structure for pure ceria and a mixture of monoclinic and tetragonal phases for pure zirconia could be identified from these XRD patterns. For the ceria-rich solid solutions, only the cubic structure was detected, whereas a mixture of tetragonal and cubic phases was detected for zirconia-rich mixed oxides. As the zirconia content in the mixed-oxide catalyst samples was increased, the XRD patterns displayed a small shift to higher values of $2\theta$, as compared to fluorite cubic $CeO_2$ (JCPDS #43-1002), and this shift is associated with the lattice contraction caused by the introduction of smaller $Zr^{4+}$ ions into the $CeO_2$ lattice. No reflections corresponding to palladium or palladium oxide phases were detected, indicating the presence of small (<4 nm) particles. The XRD patterns obtained are similar with the measurements obtained by Serrano-Ruiz et al. and Solinas et al. [12,17].

### 3.2. Reaction network

Details of the reaction network for aldol condensation/hydrogenation of 2-hexanone are explained in our previous work [9], and the main reaction pathways are shown in Fig. 4. In brief, the primary reaction pathway involves the self-coupling of 2-hexanone to yield 7-methyl-5-undecanone, as shown in Fig. 4A. In this pathway, 2-hexanone undergoes self-aldol condensation on basic sites to form an aldol alcohol, which then undergoes dehydration on acidic (or basic) sites to form an α–β unsaturated ketone, followed by hydrogenation on metal sites to yield a saturated ketone. This saturated ketone product, 7-methyl-5-undecanone, undergoes further aldol condensation with 2-hexanone (in the pathway described above) to yield a $C_{18}$ ketone. As illustrated in Fig. 4B, the equilibrated hydrogenation of the C=O group of 2-hexanone yields 2-hexanol, which can undergo dehydration over acidic sites to yield hexene, which is rapidly hydrogenated to form hexane. By analogy, 7-methyl-5-undeca-

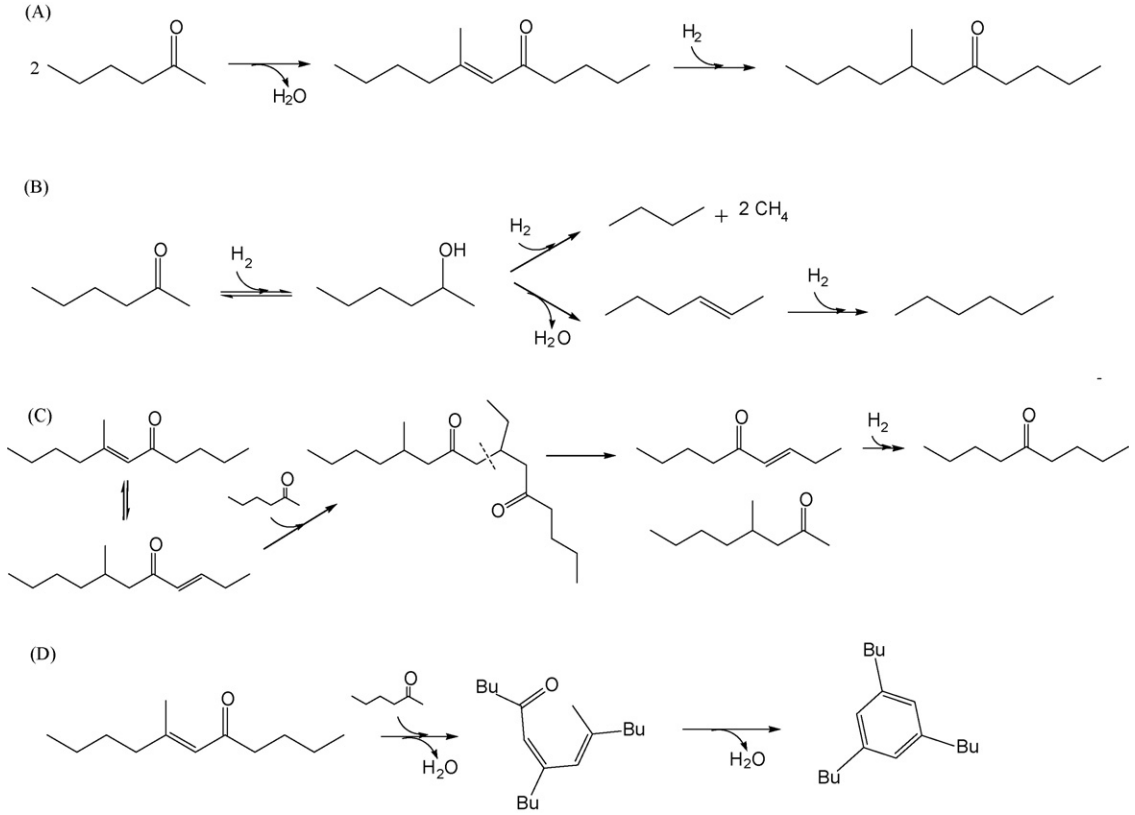


**Fig. 4.** Reactions of 2-hexanone on amphoteric oxide supported Pd catalysts.

none undergoes dehydration and hydrogenation steps to form 5-methyl undecane. Fig. 4B also shows that 2-hexanol can undergo reforming (α-scission) on palladium to form methane, butane and $CO_x$ [18,19]. The $CO_x$ species are hydrogenated to methane, and thus only small amounts of $CO_x$ species (<1% of total carbon) are detected in the gas phase. Similarly, 7-methyl-5-undecanol undergoes reforming to yield methane and 2-methyl hexane. Additionally, $C_9$ ketones may form through a C–C cleavage reaction (retro-Michael reaction) [20] of a $C_{18}$ dione (not detected in the effluent) obtained from the Michael addition of 2-hexanone to $C_{12}$ ketone [21], as demonstrated in Fig. 4C. Furthermore, the α–β unsaturated $C_{12}$ ketone can undergo cross-aldol condensation with 2-hexanone followed by a 1,6-aldol addition or aromatization to form 1,3,5-tributylbenzene, another $C_{18}$ species (Fig. 4D). This reaction is analogous to the formation of mesitylene from acetone [21]. The aromatization reaction tends to be more prevalent on acidic sites [22]. Finally, a $C_{11}$ ketone (5-undecanone) may be obtained from C–C hydrogenolysis of the methyl branch of 7-methyl-5-undecanone, yielding methane. For brevity, in the product distributions discussed in this work, species were grouped by carbon number.

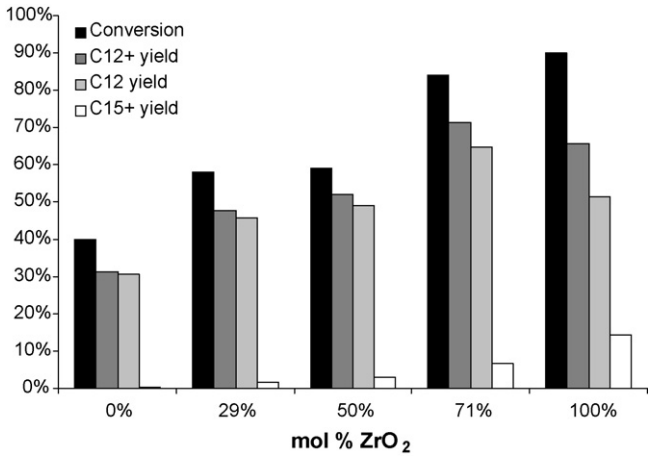


**Fig. 5.** 2-Hexanone conversion and yields for product species over $Pd/CeO_x$, $Pd/Ce_5Zr_2O_x$, $Pd/Ce_1Zr_1O_x$, $Pd/Ce_2Zr_5O_x$ and $Pd/ZrO_2$ at 623 K and 5 bar, WHSV = 1.92 $h^{-1}$. $C_{12+}$ species consist of $C_{12}$ and higher molecular weight species ($C_{15+}$). See Table 3 for detailed carbon distribution among $C_{12+}$ as well as remaining product species.

### 3.3. Aldol condensation/hydrogenation activity and selectivity over 0.25 wt% $Pd/Ce_aZr_bO_x$ catalysts

To study the effect of $CO_2$ and water on aldol condensation activity, experiments with pure 2-hexanone as the feed were first carried out for all catalysts. The activity and selectivity data for the conversion of 2-hexanone over $Pd/Ce_aZr_bO_x$ catalysts with different ceria to zirconia ratios are given in Table 3, and these results are shown graphically in Fig. 5. The 2-hexanone conversion increases with increasing $ZrO_2$ content, pure $ZrO_2$ having the highest conversion of 90%. The main product for all catalysts is the primary condensation product, 7-methyl-5-undecanone. The $C_{12}$ entry in Table 3 also includes 5-methyl-undecane, resulting from the de-oxygenation of 7-methyl-5-undecanone. For all catalysts, $C_9$ and $C_{18}$ ketones could be observed. As the quantity of acid sites is increased with increasing zirconia content, the formation of 1,3,5-tributylbenzene becomes more significant, increasing the total selectivity to $C_{18}$ species. For $Pd/Ce_2Zr_5O_x$ and $Pd/ZrO_2$, very small amounts (1–3% selectivity) of even higher molecular weight species are observed. The total selectivity of all these species is reported in the entry $C_{18+}$. Furthermore, for these two catalysts, $C_{15}$ ketones were detected, resulting from the aldol condensation of 2-hexanone with $C_9$ ketones. Some of these species could not be identified definitively using the NIST library of the GC–MS, and their identification was based on the atomic mass of the molecular ion fragment and analogous species reported for acetone condensation [21,22]. Small amounts of $C_8$ and $C_{11}$ ketones may be obtained from C–C hydrogenolysis of the methyl branch of $C_9$ and $C_{12}$ ketones.

The selectivity towards the $C_{12}$ products remains approximately constant for all the catalysts except for pure $ZrO_2$. It is possible to compare the selectivities over $Pd/Ce_2Zr_5O_x$ and $Pd/ZrO_2$ as the conversion values for the two catalysts are very similar. For pure $ZrO_2$, the selectivity shifts about 8% towards higher molecular weight species, mainly $C_{18}$ ketones and aromatics. This increase in the yield of $C_{18}$ aromatic species is due to the acidic nature of pure $ZrO_2$. The aromatization reaction is catalyzed by acid sites [22], and $ZrO_2$ has by far the highest number of acid sites as demonstrated by $NH_3$ TPD results in Table 1. Also, 2-hexanone conversion on $Pd/ZrO_2$ catalyst produces higher amounts of C–C cleavage products, such as $C_8$–$C_{11}$ ketones and lighter alkanes, at the expense of $C_{12}$ species. The large number of surface acid sites for $Pd/ZrO_2$ is responsible for the increase in selectivity towards light alkanes, mainly hexane, as the dehydration of 2-hexanol to hexene is mainly catalyzed by acid sites. As shown in Fig. 4C, a double-bond shift or isomerization is a part of the pathway for the production of $C_9$ ketones and this isomerization can also be catalyzed by acid sites [23] which are more abundant on $Pd/ZrO_2$ as compared to $Pd/Ce_2Zr_5O_x$. The increased activity of C–C hydrogenolysis to produce $C_8$ and $C_{11}$ ketones on $Pd/ZrO_2$ may result from the absence of strong metal–support interactions (SMSI). In particular, it is known in the literature that ceria exhibits strong metal–support interactions [24], and the rate of C–C hydrogenolysis can be suppressed by the presence of SMSI [25]. We have shown in our previous work [9] with temperature-programmed reduction (TPR) experiments that reduction of ceria occurs at our reduction temperatures, which is required for the onset of SMSI.

The Pd dispersions were not measured for the catalysts, except for $Pd/Ce_1Zr_1O_x$ shown in our previous work [9], because it is difficult to quantify accessible Pd sites by CO adsorption measurements in the presence of $Ce^{3+}$ formed during reduction of the catalyst by spillover of hydrogen from Pd onto the support. Serrano-Ruiz et al. measured atomic Pt/(Ce + Zr) ratios for $Pt/Ce_aZr_bO_x$ catalysts with X-ray photoelectron spectroscopy and found that the platinum dispersion decreases slightly with

**Table 3**
Product distributions from conversion of 2-hexanone over 0.25 wt% $Pd/CeO_x$, $Pd/Ce_5Zr_2O_x$, $Pd/Ce_1Zr_1O_x$, $Pd/Ce_2Zr_5O_x$ and $Pd/ZrO_2$ at 623 K and 5 bar, WHSV = 1.92 $h^{-1}$.

| Catalyst | Conversion (%) | Carbon selectivities (%) | | | | | |
|---|---|---|---|---|---|---|---|
| | | $C_{12}$ | $C_{15}$ | $C_{18+}$ | $C_9$ | $C_8$ and $C_{11}$ | Alkanes ($\leq C_7$) |
| 0.25 wt% $Pd/CeO_x$ | 40 | 77 | – | 1 | 2 | 4 | 16 |
| 0.25 wt% $Pd/Ce_5Zr_2O_x$ | 58 | 79 | – | 3 | 5 | 3 | 10 |
| 0.25 wt% $Pd/Ce_1Zr_1O_x$ | 58 | 83 | – | 5 | 2 | 2 | 8 |
| 0.25 wt% $Pd/Ce_2Zr_5O_x$ | 84 | 77 | 3 | 5 | 6 | 1 | 8 |
| 0.25 wt% $Pd/ZrO_x$ | 90 | 57 | 5 | 11 | 10 | 4 | 13 |

**Table 4**
2-Hexanone conversion and product distribution for $Pd/ZrO_2$ and $Pd/Ce_1Zr_1O_x$ at 598 K, WHSV = 256 $h^{-1}$ and 5 bar.

| Catalyst | 2-Hexanone conversion (%) | Carbon selectivities (%) | | |
|---|---|---|---|---|
| | | $C_{12}$ | $C_{18}$ | Hexane |
| 0.25 wt% $Pd/Ce_1Zr_1O_x$ | 5 | 99 | – | 1 |
| 0.25 wt% $Pd/ZrO_2$ | 39 | 98 | 2 | – |

decreasing ceria content [12]. Accordingly, we expect that the highest Pd dispersion for the $Pd/CeO_x$ catalyst. In general, the Pd dispersion does not seem to be an issue in terms of limiting the hydrogenation rate of α–β unsaturated ketone, as demonstrated by complete conversion of α–β unsaturated ketone (aldol condensation product) to the saturated ketone for all experiments, indicating that hydrogenation is a fast step in the reaction network. However, metal dispersion might be important in terms of side reactions such as hydrogenolysis and hydrogenation to yield light alkanes, and this effect might be the reason for higher selectivity towards light alkanes over $Pd/CeO_x$ even at low conversion. It is interesting to note that at the same conversion (∼40%), $Pd/ZrO_2$ produces only high molecular weight species, as shown in Table 4.

The high activities displayed by $Pd/Ce_2Zr_5O_x$ and $Pd/ZrO_2$ compared to our original catalyst $Pd/Ce_1Zr_1O_x$ are promising in terms of improving the C–C coupling yield. The conversion values for both of these catalysts are similar (84 and 90%), and the selectivity for $Pd/ZrO_2$ shows a significant shift towards higher molecular weight ketones and aromatic species and C–C cleavage products. Fig. 5 demonstrates the trend in 2-hexanone conversion, $C_{12}$ yield and $C_{12+}$ yield as the zirconia content in the mixed oxides is changed. It can be seen that while the 2-hexanone conversion and the $C_{15+}$ yield continuously increase with increasing zirconia content, the $C_{12}$ and total $C_{12+}$ yield pass through a maximum with $Pd/Ce_2Zr_5O_x$. $Pd/ZrO_2$ is the second best catalyst in terms of $C_{12}$ and total $C_{12+}$ yields. This variation in the product selectivity brings flexibility to the process, in which $Pd/Ce_2Zr_5O_x$ can be used to obtain high yields of the primary condensation product, whereas $Pd/ZrO_2$ would be preferred to increase the content of higher molecular weight species or aromatics in the product stream. It is likely that side reactions are more significant over $Pd/ZrO_2$ due to the high density of acid sites and $C_{12}$ selectivity can be increased if a higher WHSV is used. The increase in activity with increasing zirconia content in the mixed-oxide catalyst can be attributed to changes in the intrinsic properties of the catalyst, i.e. acid–base properties, and/or increased resistance to water inhibition (that is generated in aldol condensation and dehydration steps in the reaction network). These two possibilities are discussed further in the following sections.

In terms of acid–base properties, $Pd/CeO_x$ possesses weak $CO_2$ binding sites (surface $OH^-$ groups) [26]. In addition, a second peak is observed in the desorption profile at about 1000 K due to the formation of stable carbonates. As the ceria content decreases, these carbonates gradually disappear, and for all the mixed oxides, a distribution among weak, medium and strong $CO_2$ binding sites is achieved, corresponding to surface $OH^-$, $M^{x+}\cdots O^{2-}$ pairs, and low coordination $O^{2-}$ sites. These mixed oxides show higher activity than $Pd/CeO_x$. Therefore, it is probable that both surface OH– ions and $M^{x+}\cdots O^{2-}$ pairs contribute to aldol condensation activity, and the mixed oxides contain more of these sites per gram of catalyst compared to $Pd/CeO_x$. In addition, it has been reported that low coordination $O^{2-}$ sites show low activity for C–C bond formation [14,26]. This behavior is also supported by the fact that $Pd/ZrO_2$ shows high aldol condensation activity in the absence of the strong $CO_2$ binding $O^{2-}$ sites. These isolated $O^{2-}$ sites lack the acid–base site pairing that can more easily activate the C-H bond for carbanion formation [14]. Pure $ZrO_2$, on the other hand, has only surface $OH^-$ sites and $M^{x+}\cdots O^{2-}$ pairs, as shown by Bianchi et al. and Daturi et al. [15,27]. It is also possible that aldol coupling proceeds via an acid catalyzed mechanism on zirconia and zirconia-rich mixed oxides, and the high content of acidic sites contributes to the overall activity. For example, Chen et al. achieved reasonable conversions for self-condensation of acetone over $Pd/(Nb_2O_5/SiO_2)$ [28].

### 3.4. Effect of $CO_2$ and water co-feeding

To explore the effect of $CO_2$ on condensation activity over the catalysts with different compositions, we have substituted the pure hydrogen gas co-feed used above with $H_2$–$CO_2$ gas mixtures. All ceria-containing catalysts displayed significant inhibition by $CO_2$, showing yields of less than 20% to C–C coupling products. The decrease in activity for these catalysts can be correlated with the abundance of isolated $O^{2-}$ sites that strongly bind $CO_2$, as shown in $CO_2$ TPD profiles. On the other hand, $Pd/ZrO_2$ showed significant resistance to $CO_2$ poisoning (20% decrease in condensation activity), and this catalyst does not contain strong $CO_2$ binding sites. The effect of $CO_2$ co-feeding on activity and selectivity to condensation products is shown in Table 5 for all the catalysts.

In addition to $CO_2$, water is another by-product of ketonization, which we showed previously to cause a decrease by 40% in the activity for aldol condensation of 2-butanone over $Pd/Ce_1Zr_1O_x$ when a mixture containing 12 wt% water in 2-butanone was used as the feed [9]. This inhibition by water is an additional obstacle to integrating ketonization and aldol condensation/hydrogenation steps. Therefore, we have studied the effect of water on the aldol condensation activity over $Pd/ZrO_2$ by co-feeding water with 2-butanone. In these studies, 2-butanone was chosen as the reactant, because it can be saturated with a larger amount of water (∼12 wt%) than 2-hexanone, and this water content is representative of the products of ketonization. The effect of water co-feeding over $Pd/ZrO_2$ is compared in Table 6 with the effect of water addition over $Pd/Ce_1Zr_1O_x$. It can be seen that the catalytic activity decreases by about 10% for the case of $Pd/ZrO_2$ compared to a 40% decrease for $Pd/Ce_1Zr_1O_x$. The selectivity shifts slightly towards the primary condensation product, 5-methyl-3-heptanone, at the expense of secondary reaction products for both catalysts. The diminished inhibition of aldol condensation reaction by water and $CO_2$ over $Pd/ZrO_2$ makes this catalyst suitable for the integration of ketonization and aldol condensation/hydrogenation.

We now consider whether the higher activity of $Pd/ZrO_2$ might be partially or completely due to the resistance of this catalyst to water inhibition, because water is a product of aldol condensation/hydrogenation. To investigate this possibility, the activity for 2-hexanone coupling was measured over both $Pd/ZrO_2$ and $Pd/Ce_1Zr_1O_x$ at low conversions, where water generation is minimal. The reaction conditions were adjusted to 598 K, 5 bar and WHSV = 256 $h^{-1}$, such that the 2-hexanone conversion remained under 40%, and the results are presented in Table 4. The 2-hexanone conversion over $Pd/ZrO_2$ at these conditions was 39%

**Table 5**
2-Hexanone conversion and product distribution over 0.25 wt% $Pd/CeO_x$, $Pd/Ce_5Zr_2O_x$, $Pd/Ce_1Zr_1O_x$, $Pd/Ce_2Zr_5O_x$ and $Pd/ZrO_2$ with co-feeding 10 mol% $CO_2$ in $H_2$ stream at 623 K and 5 bar, WHSV = 1.92 $h^{-1}$.

| Catalyst | 2-Hexanone conversion (%) | Carbon selectivities (%) | |
|---|---|---|---|
| | | $C_{12}$ | $C_{12+}$ |
| 0.25 wt% $Pd/CeO_x$ | 4 | 34 | 0 |
| 0.25 wt% $Pd/Ce_5Zr_2O_x$ | 5 | 36 | 0 |
| 0.25 wt% $Pd/Ce_1Zr_1O_x$ | 5 | 22 | 0 |
| 0.25 wt% $Pd/Ce_2Zr_5O_x$ | 19 | 55 | 0 |
| 0.25 wt% $Pd/ZrO_x$ | 72 | 62 | 8 |

**Table 6**
2-Butanone conversion and product distribution over $Pd/ZrO_2$ and $Pd/Ce_1Zr_1O_x$ with and without the presence of water in the feed at 623 K and 5 bar, WHSV = 1.92 $h^{-1}$.

| Catalyst | Feed | 2-Butanone conversion (%) | Carbon selectivities (%) | |
|---|---|---|---|---|
| | | | $C_8$ | $C_{8+}$ |
| 0.25 wt% $Pd/Ce_1Zr_1O_x$ | 2-Butanone | 69 | 91 | 5 |
| 0.25 wt% $Pd/Ce_1Zr_1O_x$ | 12 wt% water in 2-butanone | 37 | 93 | 3 |
| 0.25 wt% $Pd/ZrO_2$ | 2-Butanone | 88 | 77 | 11 |
| 0.25 wt% $Pd/ZrO_2$ | 12 wt% water in 2-butanone | 78 | 80 | 9 |

**Table 7**
2-Hexanone and butanoic acid conversions and product selectivities for reaction of 2-hexanone containing 20 mol% butanoic acid or 20 mol% heptane over the double-bed system at 623 K and 5 bar.

| Feed (balance 2-hexanone) | Conversion (%) | | Carbon selectivities (%) | | | | | | |
|---|---|---|---|---|---|---|---|---|---|
| | 2-Hexanone | Butanoic acid | 4-Heptanone | $C_{12}$ | $C_{15}$ | $C_{18+}$ | $C_9$ | $C_8$ and $C_{11}$ | Alkanes ($\leq C_7$) |
| 20 mol% heptane | 76 | – | – | 51 | 5 | 11 | 9 | 5 | 19 |
| 20 mol% butanoic acid | 75 | 100 | 11 | 45 | 5 | 5 | 12 | 7 | 14 |

whereas it was only 5% over $Pd/Ce_1Zr_1O_x$. At these low conversions both catalysts showed high selectivities towards the primary condensation product, 7-methyl-5-undecanone. These results demonstrate that $Pd/ZrO_2$ is still significantly more active compared to $Pd/Ce_1Zr_1O_x$ when water inhibition is minimized. Even though the resistance to water inhibition might play a role for the performance of $Pd/ZrO_2$ at high conversions, it is not the only cause for the enhanced activity of $Pd/ZrO_2$ as compared to $Pd/Ce_1Zr_1O_x$.

### *3.5. Integration of ketonization and aldol condensation/hydrogenation reactions in a single reactor, double bed system for a simulated feed mixture*

The results of this study involving different compositions of ceria-zirconia mixed-oxide catalysts indicate that $Pd/ZrO_2$ is the preferred catalyst to be used for integration of ketonization and aldol condensation/hydrogenation reactions in a single reactor system. $Pd/ZrO_2$ has high activity and it is resistant to inhibition by $CO_2$ and water. To test the applicability of a double bed system, a 20 mol% mixture of butanoic acid in 2-hexanone was used as the feed. Before using the double bed set up, the following conditions for complete conversion of butanoic acid over $Ce_1Zr_1O_x$ in the ketonization step were found: 623 K and 5 bar, and WHSV = 1.92 $h^{-1}$. Under these conditions, butanoic acid reacted with 100% conversion to the ketonization product, 4-heptanone, and 6% of the 2-hexanone was converted to yield the primary aldol condensation product – an unsaturated $C_{12}$ ketone – and C–C cleavage products ($C_{11}$ and $C_9$ ketones). The double bed system was then set up by adding a downstream $Pd/ZrO_2$ catalyst to achieve aldol condensation/hydrogenation following the ketonization step. The reaction system was carried out at 623 K and 5 bar, with $H_2$ co-feed for a liquid feed of 2-hexanone containing 20 mol% butanoic acid, compared to a liquid feed of 2-hexanone containing 20 mol% heptane (as an inert species). Results obtained for these two runs are presented in Table 7. The heptane containing mixture was used in a control experiment to test for the effects of $CO_2$ and water generated by ketonization. $C_{12}$ species include 7-methyl-5-undecanone and 5-methyl-undecane. $C_{18+}$ species include the condensation product of 7-methyl-5-undecanone and 2-hexanone, 1,3,5-tributylbenzene and a small fraction of higher molecular weight species. $C_{15}$ ketone is the condensation product of 2-hexanone and $C_9$ ketone. $C_8$ and $C_{11}$ ketones are obtained from C–C hydrogenolysis reactions as discussed previously. Finally, lighter alkanes are obtained from dehydration/hydrogenation of the feed, and reforming reactions of the alcohols formed within the reaction network. It can be seen that there is little difference between the activity and selectivity values for the two runs. These results show that $Pd/ZrO_2$ is resistant to the $CO_2$ and water generated in the ketonization step for this simulated feed mixture and that the double bed system can be successfully implemented.

## 4. Conclusions

Production of liquid transportation fuels by catalytic upgrading of hydrophobic mixtures of mono-functional intermediates obtained from carbohydrates over Pt-Re/C can be achieved by the integration in a single reactor of ketonization and aldol condensation/hydrogenation steps. With this integration of steps, the energy consumption as well as reactor infrastructure associated with cooling and re-heating the products obtained from ketonization prior to the aldol condensation/hydrogenation step can be eliminated. For this integration to be realized, the catalyst for aldol condensation must be resistant to inhibition by the $CO_2$ and water produced in the ketonization step. We have found that $Pd/Ce_2Zr_5O_x$ and $Pd/ZrO_2$ show high activity for aldol condensation of 2-hexanone, a representative ketone produced from carbohydrates over Pt-Re/C. Formation of $C_{12}$ products was predominant on both catalysts, and secondary reaction products, such as $C_{18}$ ketones and aromatic species, were produced with higher selectivities over $Pd/ZrO_2$, likely due to the high surface acidity of this catalyst. The inhibiting effect of $CO_2$ on the rate of aldol condensation was significant over all compositions of ceria-zirconia mixed-oxide catalysts, as well as $Pd/CeO_x$. However, $Pd/ZrO_2$ was found to be substantially more resistant to $CO_2$ inhibition. The effect of water co-feeding was investigated over $Pd/ZrO_2$, in comparison with $Pd/Ce_1Zr_1O_x$, and it was found that $Pd/ZrO_2$ was also more resistant to water inhibition compared to $Pd/Ce_1Zr_1O_x$. With these promising catalytic properties of $Pd/ZrO_2$, a double bed system consisting of $Ce_1Zr_1O_x$ (for ketonization) followed by $Pd/ZrO_2$ (for aldol condensation) was successfully implemented to achieve the combined C–C coupling of carboxylic acids and ketones, as illustrated with a simulated mixture of 20 mol% butanoic acid in 2-hexanone.

## Acknowledgements

This work was supported in part by the U.S. Department of Energy Office of Basic Energy Sciences, and by the DOE Great Lakes Bioenergy Research Center (www.greatlakesbioenergy.org), which is supported by the U.S. Department of Energy, Office of Science, Office of Biological and Environmental Research, through Cooperative Agreement DE-FC02-07ER64494 between The Board of

Regents of the University of Wisconsin System and the U.S. Department of Energy.

## References

[1] E.L. Kunkes, D.A. Simonetti, R.M. West, J.C. Serrano-Ruiz, C.A. Gaertner, J.A. Dumesic, Science 322 (2008) 417.
[2] O. Nagashima, S. Sato, R. Takahashi, T. Sodesawa, J. Mol. Catal. A 227 (2005) 231.
[3] A.A. Nikolopoulos, B.W.L. Jang, J.J. Spivey, Appl. Catal. A 296 (2005) 128.
[4] R.M. West, Z.Y. Liu, M. Peter, J.A. Dumesic, ChemSusChem 1 (2008) 417.
[5] R.M. West, E.L. Kunkes, D.A. Simonetti, J.A. Dumesic, Catal. Today 5 (2008).
[6] G. Torres, C.R. Apesteguia, J.I. DiCosimo, Appl. Catal. A 317 (2007) 161.
[7] S. Abello, D.V. Shankar, J. Perez-Ramirez, Appl. Catal. A 342 (2008) 119.
[8] Y. Kamimura, S. Sato, R. Takahashi, T. Sodesawa, T. Akashi, Appl. Catal. A 252 (2003) 399.
[9] E.L. Kunkes, E.I. Gurbuz, J.A. Dumesic, J. Catal. 206 (2009) 236.
[10] V.K. Diez, J.I. DiCosimo, C.R. Apesteguia, Appl. Catal. A 345 (2008) 143.
[11] J.I. DiCosimo, V.K. Diez, M. Xu, E. Iglesia, C.R. Apesteguia, J. Catal. 178 (1998) 499.
[12] J.C. Serrano-Ruiz, J. Luettich, A. Sepulveda-Escribano, F.R. Reinoso, J. Catal. 241 (2006) 45.
[13] B.E. Spiewak, J. Shen, J.A. Dumesic, J. Phys. Chem. 99 (1995) 17640.
[14] J.I. DiCosimo, C.R. Apesteguia, M.J.L. Gines, E. Iglesia, J. Catal. 190 (2000) 261.
[15] M. Daturi, C. Binet, J. Lavalley, A. Galtayries, R. Sporken, Phys. Chem. Chem. Phys. 1 (1999) 5717.
[16] S.M. DeLima, A.M. Silva, U.M. Graham, G. Jacobs, B.H. Davis, L.V. Mattos, F.B. Noronha, Appl. Catal. A 352 (2009) 95.
[17] V. Solinas, E. Rombi, I. Ferino, M.G. Cutrufello, G. Colon, J.A. Navio, J. Mol. Catal. A: Chem. 204–205 (2003) 629.
[18] R. Alcala, M. Mavrikakis, J.A. Dumesic, J. Catal. 218 (2003) 178.
[19] R.D. Cortright, R.R. Davda, J.A. Dumesic, Nature 418 (2002) 964.
[20] J. Wang, T. Li, Collect. Czech. Chem. Commun. 64 (1998) 107.
[21] S. Lippert, W. Baumann, K. Thomke, J. Mol. Catal. 69 (1991) 199.
[22] G.S. Salvapati, K.V. Ramanamurty, M. Janardanarao, J. Mol. Catal. 54 (1989) 9.
[23] I. Coleto, R. Roldan, C. Jimenez-Sanchidrian, J.P. Gomez, F.J. Romero-Salguero, Catal. Today, in press.
[24] M. Abid, V. Paul-Boncour, R. Touroude, Appl. Catal. A 297 (2006) 48.
[25] S.A. Stevenson, G.B. Raupp, J.A. Dumesic, S.J. Tauster, R.T.K. Baker, in: S.A. Stevenson, J.A. Dumesic, R.T.K. Baker, E. Ruckenstein (Eds.), Metal–Support Interactions in Catalysis, Sintering, and Redispersion, Van Nostrand Reinhold Company, New York, 1987, pp. 55–75.
[26] J.I. DiCosimo, G. Torres, C.R. Apesteguia, J. Catal. 208 (2002) 114.
[27] D. Bianchi, T. Chafik, M. Khalfallah, S.J. Teichner, Appl. Catal. A 112 (1994) 219.
[28] Y.Z. Chen, B.J. Liaw, H.R. Tan, K.L. Shen, Appl. Catal. A 205 (2001) 61.